MOHeaCAN

ESTIMATING THE GLOBAL OCEAN HEAT CONTENT AND THE EARTH ENERGY IMBALANCE PRODUCTS FROM SPACE

ALGORITHM THEORETICAL BASIS DOCUMENT

	Name	Organization	Date	Visa
Written by:	Florence Marti Michaël Ablain Rémi Jugier Robin Fraudeau Victor Rousseau	Magellium	09/09/2020	
	Benoit Meyssignac Alejandro Blazquez	LEGOS		
Checked by:	Michaël Ablain	Magellium	09/09/2020	
Approved by:	Joël Dorandeu	Magellium	09/09/2020	

Document reference:	MOHeaCAN-DT-001-MAG_ATBD
Edition.Revision:	1.5
Date Issued:	08/12/2021
Data Set Version:	v3-0 (date of release: 08/12/2021)

Document evolution sheet

Ed.	Rev.	Date	Purpose evolution	Comments
1	0	02/03/2019	Creation of document	
1	1	09/09/2020		Feedback from MTR
1	2	13/10/2020	Release of first product version (v1-0)	Consideration of observations and requests from ESA's first review Integration of a regional grid of GIA in altimetry data (sections 2.7 and 3.5.2.3) Update of the comments/limitations section 3.5.4.3
1	3	26/04/2021	Release of new product version (v2-0)	Use of a new ocean mass solutions ensemble.
1	4	09/09/2021	Release of new product version (v2-1)	Addition of the elastic correction for the recent melting and contributions from other climate reservoirs to EEI (β coefficient).
1	5	08/12/2021	Release of new product version (v3-0)	Add gap filling algorithm on Ocean Mass data (section 3.5.3.4) Use of a new ocean mass solutions ensemble (V1.5) (section 2.1) Use of new C3S altimetry data version (vDT2021) (section 2.2) New format of OHC-EEI netCDF file (splitted in 2 different files) (section 3.4) New method for compute temporal derivative of GOHC (section 3.5.10.3)

Contents

List of figures

List of tables

1. Introduction

1.1. Executive summary

Since the industrial era, anthropogenic emissions of greenhouse gases (GHG) in the atmosphere have lowered the total amount of infrared energy radiated by the Earth towards space. Now the Earth is emitting less energy towards space than it receives radiative energy from the sun. As a consequence there is an energy imbalance (EEI) at the top of the Atmosphere (Hansen et al., 2011; Trenberth et al., 2014). It is essential to estimate and analyse the Earth Energy Imbalance (EEI) if we want to understand the Earth's changing climate. Measuring the EEI is challenging because the EEI is a globally integrated variable whose variations are small (of the order of several tenth of $W.m^{-2}$, von Schuckmann et al. (2016) compared to the amount of energy entering and leaving the climate system (of ~340 $W.m^{-2}$, (L'Ecuyer et al., 2015)). An accuracy of <0.3 $W.m^{-2}$ at decadal time scales is necessary to evaluate the long term mean EEI associated with anthropogenic forcing. Ideally an accuracy of <0.1 $W.m^{-2}$ at decadal time scales is desirable if we want to monitor future changes in EEI which shall be a non-controversial science based information used by the GHG mitigation policies (Meyssignac et al., 2019).

EEI can be estimated by an inventory of heat changes in the different reservoirs - the atmosphere, the land, the cryosphere and the ocean. As the ocean concentrates the vast majority of the excess of energy (~90%) in the form of heat (von Schuckmann et al., 2020), the global Ocean Heat Content (OHC) places a strong constraint on the EEI estimate.

In the MOHeaCAN project, the OHC is estimated from the measurement of the thermal expansion of the ocean based on differences between the total sea-level content derived from altimetry measurements and the mass content derived from gravimetry data (noted space geodetic or "Altimetry-Gravimetry" approach). This space geodetic approach provides consistent spatial and temporal sampling of the ocean, it samples nearly the entire global oceans, except for polar regions, and it provides estimates of the OHC over the ocean's entire depth. It complements the OHC estimation from Argo (direct measurement of in situ temperature based on temperature/salinity profiles).

MOHeaCAN project's objectives were to develop novel algorithms, estimate realistic OHC uncertainties thanks to a rigorous error budget of the altimetric and gravimetric instruments, in order to reach the challenging target for the uncertainty quantification of 0.3 W. m^{-2} which then allow our estimate to contribute to better understand the Earth's climate system.

1.2. Scope and objectives

This document is the Algorithm Theoretical Basis Document (ATBD) of the MOHeaCAN product initially supported by ESA and now supported by CNES. This ATBD is dedicated to the description and justification of the algorithms used in the generation of the **OHC and EEI products**. A scientific validation of the OHC-EEI MOHeaCAN product is described in Marti et al. (2021).

The calculation of OHC and EEI products is divided in several steps as presented in the following figure (Figure 1). The first step is to process the input data from the altimetry and spatial gravimetry measurements to allow their differences to be calculated in the next step. Then the processing of the OHC at the global and regional levels can thus be carried out in two distinct stages with certain dependencies as will be discussed later. The EEI is obtained from the global Ocean Heat Uptake (GOHU) which is derived from the global OHC. The last step consists in computing uncertainties of OHC and EEI products, propagating the errors from input data until the final products. This stage is performed on OHC and EEI resulting from the computation at global level only.

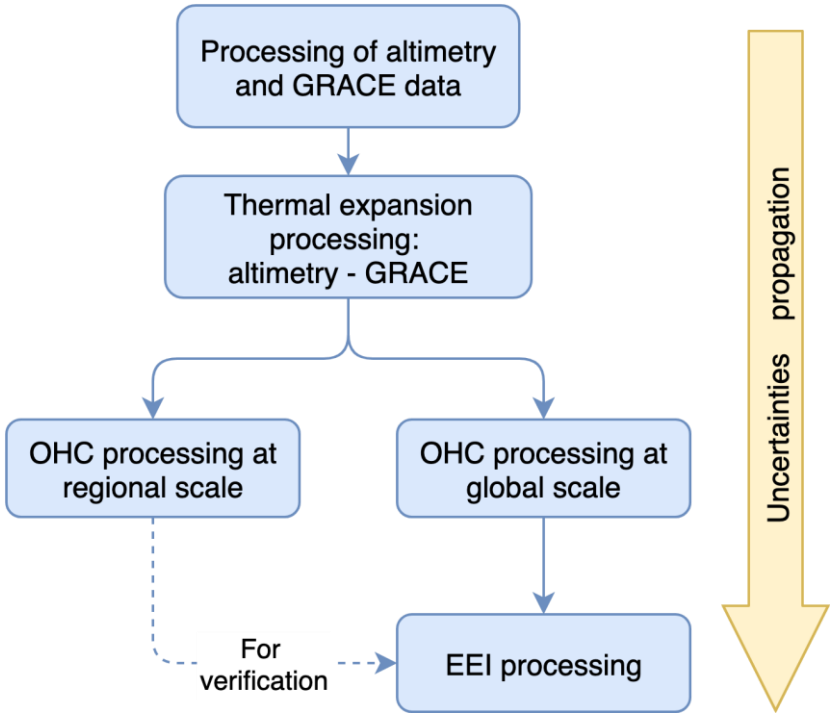

Figure 1 *: MOHeaCAN processing chain steps for the estimation of OHC and EEI and its uncertainties*

This ATBD is divided into 3 sections. We first describe the input data for the processing chain, mainly altimetry and gravimetry observations. We then explain how the OHC and the EEI are calculated before presenting the uncertainty propagation methodology in the last section.

1.3. Document structure

In addition to this introduction, the document is organised as follows:

- Section 2 provides the description of the input data of the MOHeaCAN processing chain.
- Section 3 provides a detailed description and justification of every step in the OHC and EEI computation.
- Section 4 provides a detailed description and justification of the uncertainty propagation methodology until the final OHC-EEI products.

1.4. Reference documents

Id.	Ref.	Description
RD1	-	C3S data store: https://cds.climate.copernicus.eu/
RD2	D3.SL.1-v2.0_PUGS_of_v2DT2021_SeaLevel_products_v1.1_APPROVED_Ver1.pdf	Product product user manual of sea level daily gridded data for the global ocean from 1993 to present from Copernicus Climate Change Service (C3S): https://datastore.copernicus-climate.eu/documents/satellite-sea-level/vDT2021/D3.SL.1-v2.0_PUGS_of_v2DT2021_SeaLevel_products_v1.1_APPROVED_Ver1.pdf
RD3	D1.SL.2-v2.0_ATBD_of_v2DT2021_SeaLevel_products_v1.1_APPROVED_Ver1.pdf	Algorithm Theoretical Basis Document of sea level daily gridded data for the global ocean from 1993 to present from Copernicus Climate Change Service (C3S): : https://datastore.copernicus-climate.eu/documents/satellite-sea-level/vDT2021/D1.SL.2-v2.0_ATBD_of_v2DT2021_SeaLevel_products_v1.1_APPROVED_Ver1.pdf
RD4	ftp://ftp.legos.obs-mip.fr/pub/soa/gravimetrie/grace_legos/V1.5/	Ensemble of the ocean mass solutions provided by (Blazquez et al., 2018) on LEGOS FTP site.
RD5	https://grace.jpl.nasa.gov/data/data-updates/	Jet Propulsion Laboratory (NASA) website dedicated to Gravity recovery and climate experiment, GRACE and GRACE-FO missions.
RD6	https://www.aviso.altimetry.fr/en/data/products/ocean-indicators-products/mean-sea-level.html	AVISO indicator: global mean sea level time-series from altimetry reference missions

Table 1 *: List of reference documents*

1.5. Terminology

Abbreviation/acronym	Description
ATBD	Algorithm theoretical basis document

Argo	International program that uses profiling floats deployed worldwide to observe ocean properties such as temperature and salinity.
AVISO	Satellite altimetry data platform developed by the French national centre for space studies (CNES)
C3S	Copernicus Climate Change Service
CMEMS	Copernicus Marine Environment Monitoring Service
EEH	Expansion efficiency of heat
EWH	Equivalent water height
FTP	File transfer protocol
GIA	Glacial isostatic adjustment
GOHC	Global ocean heat content
GOHU	Global ocean heat uptake
GMOM	Global mean of ocean mass
GMSL	Global mean sea level
GMSSL	Global mean steric sea level
IEEH	Integrated expansion efficiency of heat
LEGOS	Laboratoire d'Etudes en Géophysique et Océanographie Spatiale
OLS	Ordinary least square
OM	Ocean mass
PUM	Product user manual
RD	Reference document
SL	Sea level
SLA	Sea level anomaly
SSL	Steric sea level
TBC	To be completed
TBD	To be defined
TOA	Top-of-atmosphere

Table 2 *: List of abbreviations and acronyms*

2. Input data

2.1. Overview

The following section describes the different datasets used for the computation of the ocean heat content grids and the Earth energy imbalance. They include dynamic data, varying over time, as the observations of sea level or mass variations as well as static data like the thermal expansion coefficient. These inputs are mostly 2D data given on the entire globe. However, their spatial availability is different and may vary over time.

The origin and format of each dataset are described in a dedicated subsection. The limitations and errors associated with the sea level change, mass change and thermal expansion datasets are also presented.

2.2. Dynamic data: ocean mass

2.2.1. Description

Ocean mass (OM) estimates are derived from gravimetric measurements. GRACE and GRACE Follow On (GRACE-FO) missions provide the Earth's surface mass changes from 04/2002 to 12/2020. As the GRACE data are impacted by different error sources (Blazquez et al., 2018; Meyssignac et al., 2019), we used an ensemble approach in order to average the errors and also to evaluate the uncertainty in ocean mass.

Blazquez et al., 2018 provided an ensemble of OM solutions derived from GRACE. Spherical harmonics solutions from various processing centres have been considered as those from the Center for Space Research (CSR), the Jet Propulsion laboratory (JPL), the Deutsches GeoForschungsZentrum (GFZ), the Technische Universität Graz (TUG), the Groupe de Recherche en Géodésie Spatiale (GRGS), and the International Combination Service for Time-variable Gravity Fields (COST-G). These solutions cannot be directly used to estimate the ocean mass; they need first to be post-processed (Wahr et al., 2004). The post-processing parameters includes (i) the addition of independent estimates of the degree 1 and degree 2 order 0 spherical harmonics (as these harmonics are not observable by GRACE), (ii) a filtering for correlated errors that maps into characteristic north-south stripes, (iii) a correction for the large land signals (from hydrology or glaciers) that can 'leak' into the ocean because of the limited spatial resolution of GRACE, and (iv) a correction for glacial isostatic adjustment (GIA). Blazquez et al., 2018 applied a range of state-of-the-art post-processing parameters to get a spread of GRACE estimates of the ocean mass. A time mean over 2005–2015 is removed from all GRACE solutions to compute anomalies.

For this study we used an update of the ensemble from Blazquez et al., 2018, including the GRACE-FO mission and considering datasets from different processing centres and different post-processing parameters, including an earthquake correction. The version v1.5 that is used includes new improvements:

- A priori fields includes Lakes Glaciers only region with large loss of mass from Antarctica & Greenland.

- Earthquakes: Tang correction at 2000 km for Sumatra & 1000 km for the others.
- Land/ocean leakage performs after the other corrections and only for the residual signal.

This led to a new ensemble of 216 solutions.

OM data is described and available in NetCDF format file on the following LEGOS FTP [Table 1, RD4]. Its content is described below:

- Ensemble of 216 OM solutions and its ensemble mean (Blazquez et al., 2018)
  - units: m equivalent water height (EWH)
  - spatial resolution: 1° x 1°
  - temporal resolution: monthly
  - temporal availability: August 2002 - December 2020
  - version: v1.5

2.2.2. Comments/limitations

As explained in Blazquez et al., 2018, the combination of the different raw solutions (from processing centres) with the different post-processing parameters (geocenter motion correction, filtering techniques, leakage and GIA corrections) leads to an ensemble which is assumed to cover a significant part of the uncertainty range of GRACE ocean mass estimates.

For this reason, the entire 216 solutions ensemble is used to estimate the OM change uncertainties at global scale (see section 4.4.2).

2.3. Dynamic data: sea level

2.3.1. Description

Sea level (SL) is estimated from altimetry. We used the sea-level products distributed by the Copernicus Climate Service (C3S) based on the recommendation of the ESA CCI sea level project. These products are obtained using a stable altimeter constellation (two-satellites) and homogeneous corrections and standards in time. Consequently, they allow monitoring long-term evolution of the sea level for climate change studies.

C3S provides the sea level anomaly (SLA) around a mean sea surface (MSS) above the reference mean sea-surface computed over 1993-2012, or in other words, the total SL changes [Table 1, RD2]. Data is available in NetCDF format files on the C3S data store [Table 1, RD1]. The main characteristics of SLA grids are:

- spatial resolution: 0.25° x 0.25°
- temporal resolution: daily
- temporal availability: altimetry era, January 1993 - December 2020
- units: m
- version: vDT2021

More information is available in the product user manual of C3S [RD2].

2.3.2. Comments/limitations

C3S data result from the most up-to-date standards (altimeter standards, geophysical corrections) whose timeliness is compatible with the C3S production planning and most of them follow the recommendations of the ESA Sea Level CCI project. They are submitted to a rigorous validation process.

However, these data are affected by errors like any spatial measurements. The full description of these errors was described by Ablain et al., 2015, 2019. In this study, a variance-covariance matrix dedicated to the description of the global mean sea level (GMSL) error was provided (Ablain et al., 2018). This error matrix is also well adapted to the description of C3S data measurements because the GMSL errors are the same (similar altimeter standards). It has therefore been used as an input for the error propagation purpose in this project (see section 4 devoted to this topic).

2.4. Static data: expansion efficiency of heat

2.4.1. Description

The expansion efficiency of heat (EEH) expresses the change in ocean density due to heat uptake. As a matter of fact it represents the ratio of the thermosteric sea level change over the heat content change under a given heat uptake. The EEH is dependent on temperature, salinity and pressure (Russell et al., 2000). Thus, integrated over the total water column, the EEH is supposed to vary with latitude along with the variations of integrated salinity, temperature and pressure. In time, the change in EEH is supposed to be negligible

So far the global EEH (called 'ε' hereafter) has been calculated from hydrographic data based on expendable bathythermograph and CTD (Kuhlbrodt and Gregory, 2012; Levitus et al., 2009; Melet and Meyssignac, 2015; Russell et al., 2000).

2.4.1.1. Global value of the EEH

As an extensive variable, the global EEH value cannot be retrieved directly from regional values as a simple average for instance. For the calculation of EEH at global scale the ratio between the thermosteric component of the GMSL change and GOHC change is done. These monthly ratios are averaged over time (2005-2015), then over 11 Argo solutions to provide a global EEH estimate representative of the 0–2000 m ocean column. Details can be found in Marti et al., 2021:

$$\varepsilon = 0.145 \pm 5.5.10^{-4}\, m.YJ^{-1}$$

Where $1\,YJ = 10^{24}\,J$. For information, values of the global EEH are available in the literature. Kuhlbrodt and Gregory (2012), as Levitus et al., 2012 estimated ε at 0.12 ± 0.01 m.YJ^{-1} representative of the 0–2000 m ocean column over 1955–2010. Alternate observational estimates by Church et al., 2011 for the full ocean depth over 1972–2008 suggest ε = 0.15 ± 0.03 m.YJ^{-1}, with larger uncertainties.

2.4.1.2. Regional values of the integrated EEH

At a regional scale, the EEH has never been calculated. To explain this, it occurs that the OHC change over an entire water column can be null whilst the thermosteric component of the SSL change is not. In such a situation, the EEH is not defined and cannot be calculated. A way to avoid this issue is to consider the integrated expansion efficiency of heat (IEEH) instead of the EEH. The IEEH expresses the ratio of the thermosteric component of the SSL over the OHC. In the framework of this project, IEEH values at regional scales are provided at a 3-degree resolution 2D grid from monthly 3D in situ temperature and salinity fields based on 11 various Argo solutions. Details can be found in Marti et al., 2021. These values are representative of the 0–2000 m ocean column over the 2005-2016 period; marginal seas are excluded. The value of the IEEH for each cell is the temporal mean of the ratio between the thermosteric SSL component and the OHC over 2005-2016, for exactly the same cell. The final IEEH grid corresponds to the mean of the IEEH results obtained with the 11 different Argo solutions. Data is available in NetCDF format file (units: $m.J^{-1}$, spatial resolution: 3° x 3°).

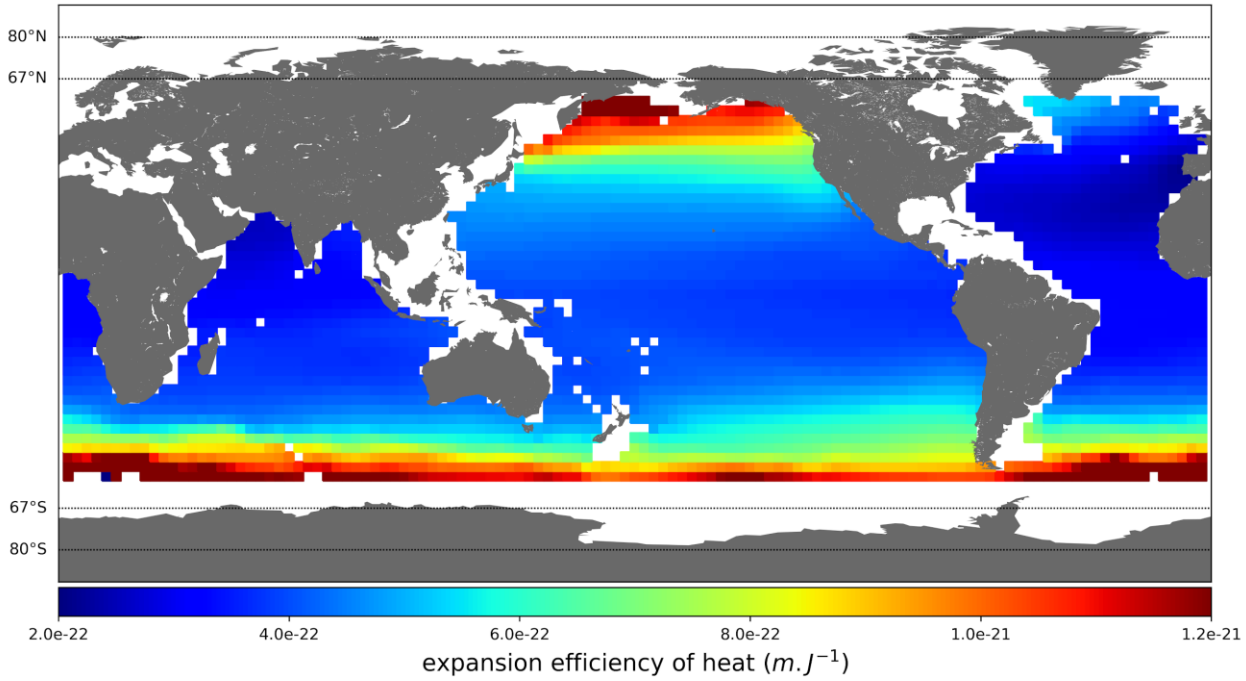

Figure 2 *: Integrated Expansion Efficiency of Heat (IEEH) coefficients ($m.J^{-1}$) at regional scale (3x3 degrees) provided by Marti et al., 2021.*

2.4.2. Comments/limitations

To assess the uncertainties on the OHC and EEI derived from data at global level, the uncertainty on the global EEH is required. The one given in Section 2.4.1.2 is the standard deviation of the 11 global EEH estimates computed over 2005-2016 (Marti et al., 2021). It is significantly lower than errors obtained by Kuhlbrodt and Gregory (2012) and Church et al. (2011).

2.5. Static data: water ratio

When manipulating data at regional scales, it is necessary to know the proportion of ocean in each cell for grid's downsampling or deriving the global mean for instance.

A water ratio grid is computed from distance to coast information and provides the part of water surface in each cell of the grid between 0 and 1. Distance to coast data are provided by the NASA Goddard Space Flight Center (GSFC) Ocean Color Group and given on a 0.01° resolution grid.

2.6. Static data: grid cells area

When manipulating data at regional scales, it is necessary to know the area of each cell for grid's downsampling or deriving the global mean for instance. The surface is computed for each grid cell taking the Earth oblateness into consideration.

2.7. Static data: global isostatic adjustment for altimetry data

Grids of sea level provided by C3S do not take in consideration the global isostatic adjustment (GIA) process in response to the melting of the Late Pleistocene ice sheets. However, this effect needs to be corrected in sea level estimates as it does not reflect the ocean's response to recent climate change. At global scale, a -0.3 mm/yr (e.g. AVISO indicator [Table 1, RD6]) correction is usually applied by the different groups providing the GMSL time series. GIA contains also regional variations that must be corrected. It is still an area of active research, and then several GIA grids expressed as trends in lithospheric height change (in mm/year) are available in the litterature. The same GIA correction used in the recent study (Prandi et al., 2020) for an estimation of the sea level trends uncertainties at local scale has been applied. It is an ensemble mean of the regional GIA results for model ICE-5G, with various viscosity profiles (27 profiles). The methodology is also described in Spada and Melini, 2019. The average GIA value over oceans from this 27 solution ensemble is 0,33 $mm.yr^{-1}$ closely matching the value of $-0.3\ mm.yr^{-1}$, generally adopted as a rule of thumb to correct the altimetric absolute sea-level trend for the effects of past GIA.

An additional correction is considered to take into account the ocean bottom deformation due to present-day mass redistribution. This correction GRD (changes in Earth Gravity, Earth Rotation and viscoelastic solid-Earth Deformation) has been evaluated at 0.1 mm/yr during the altimetry area (1993-2014), (Frederikse et al., 2017). We have applied this correction only on sea level

observations because this effect has no impact on the gravimetric data. The constant value is used in the regional computation.

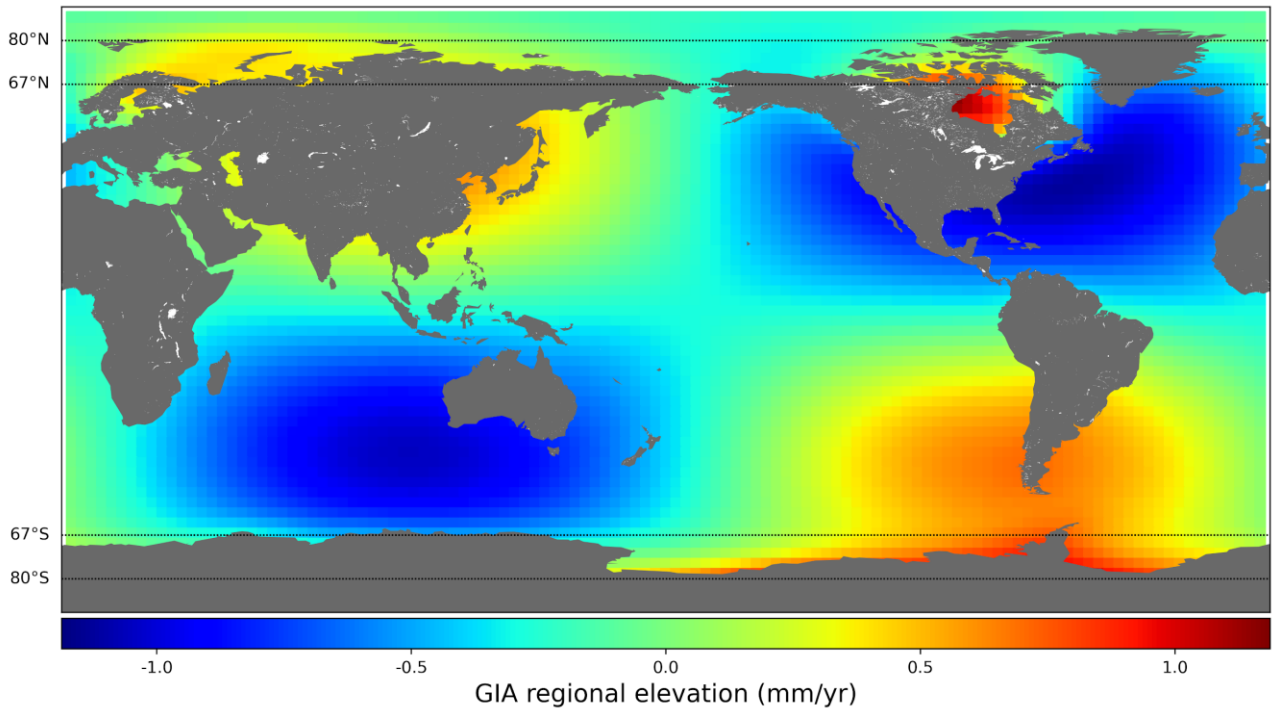

Figure 3 *: Regional grid of the GIA correction applied to altimetry sea level grids in MOHeaCAN processing chain (from Spada and Melini, 2019)*

3. OHC and EEI processing chain

3.1. Outline

In the MOHEACAN processing chain, the EEI is deduced from the Global Ocean Heat Uptake (GOHU) which is a very good approximation since the oceans store 90% of the heat kept by the Earth system (von Schuckmann et al., 2020).

The GOHC is itself estimated from space data from altimetry and gravimetry missions (GRACE and GRACE-FO). In the MOHeaCAN project, the GOHC can be obtained in 2 different and consistent ways, either from regional time series or from global mean time series. As described macroscopically in the figure below, each of these two approaches provide access to the same EEI . However, they have complementary interests. On one hand, the global approach allows the uncertainties of the global mean sea level and ocean mass (GMSL and GMOM respectively) time series to be propagated to the GOHC time series and the EEI . The state of the art on the precise knowledge of these uncertainties does not allow us for the moment to carry out this methodology of uncertainties propagation at regional scales. On the other hand, the regional approach allows us to know the 2D distribution of ocean heat content, which is essential for understanding climate change at regional scales.

As the OHC is computed from altimetry and gravimetry spatial observations, its spatial and temporal characteristics depend on these measurements. However the derived OHC characteristics are only limited by gravimetry observations both at spatial and temporal scales. Indeed, the effective temporal and spatial resolutions of GRACE(-FO) products is 1 month and 300 km against about 10-days at about 100 km for level-4 altimetry products. Therefore the regional OHC grids in the MOHeaCAN project have been defined at 3°x3° resolution and on a monthly basis. The EEI is derived from the temporal derivative of the GOHC after filtering-out the high-frequency signals lower than 3 years in order to assess the long-term EEI variable.

For reminder, the variables noted SL and OM in this document are not absolute quantities but anomalies with respect to a reference (see sections 2.2.1 and 2.3.1). SSL and OHC variables and the global variables (GMSL, GMOM, GMSSL, GOHC) are therefore also anomalies.

The Figure 4 below describes the MOHEACAN processing chain with its main algorithms for generating OHC/EEI data from input altimetry and gravimetry data. The following subsections describe the algorithms developed in detail.

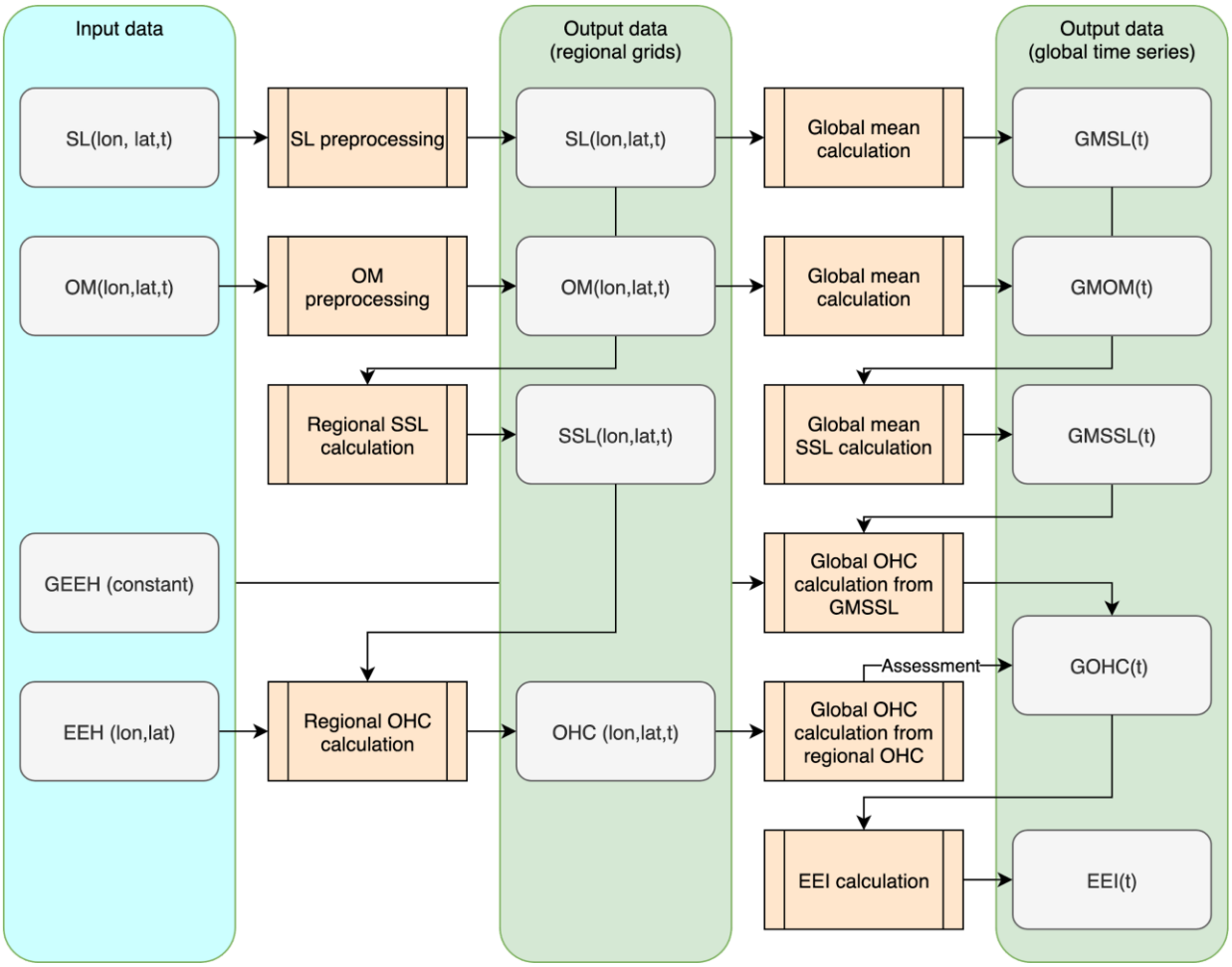

Figure 4 *: Overview of the MOHeaCAN processing chain separating regional and global mean time series. Variables are given with their dimensions (lon: longitude, lat: latitude, t: time)*

3.2. Basic underlying assumptions

The OHC is a good proxy for EEI

As the majority of the excess of energy held back in the Earth system is stored by the oceans (90%), the ocean heat content is assumed to be a reliable gauge to monitor the energy budget of the system. In this project, we assume the land, atmosphere and cryosphere reservoirs contribute 10% to the energy storage at large time scales.

The space geodetic methodology allows the estimation of the steric sea level changes due to thermal expansion (thermosteric) and salinity variations (halosteric)

Variability in ocean salinity yields sea level changes mainly at regional scales, at global scale the ocean salinity variations can be neglected.

The thermal expansion efficiency (EEH) does not change over time

EEH is known to vary spatially, over ocean depth and over time, however climate models suggest changes in the global EEH are likely negligible on decadal time scales (Meyssignac et al., 2019). Consequently, the estimated IEEH regional map and global value of EEH (Section 2.4) are assumed to be relevant over the study period (see Section 3.4).

The EEI is defined as the flux of excess/deficit of energy measured on top of the atmosphere

OHC and EEI variables are defined in relation to a reference surface, localised 20 km above the sea level. This reference level has been assumed for defining satellite-based TOA fluxes (Loeb et al., 2018).

3.3. Input data

The MOHeaCAN processing chain to compute OHC and EEI variables is configured to use the following input data, described in Section 2.

- OM gridded data (spatial resolution: 1°x 1° - temporal resolution: monthly)
- SL gridded data (spatial resolution: 0.25°x 0.25° - temporal resolution: daily)
- Global EEH value
- IEEH gridded data (spatial resolution: 3°x 3°)
- land mask (spatial resolution: 1° x 1°)

3.4. Output data

The MOHeaCAN main product contains the OHC-EEI produced by the processing chain and described in Figure 4 for each month from August 2002 to December 2020:

- Global OHC time data series
- EEI for GOHC low-pass 3 year filtered period
- Variance-covariance matrices of GOHC and EEI
- GOHC and EEI quality flag (cf. paragraph 3.5.3.4)

The format of MOHeaCAN product is described in detail in the MOHeaCAN product user manual (PUM).

An additional product is available upon request which contain other variables, mainly the intermediate variables (cf PUM).

3.5. Retrieval methodology

3.5.1. Overview

The algorithms applied in the MOHeaCAN processing chain are described in the following subsections in agreement with Figure 4:

- the preprocessing of regional SL grids
- the preprocessing of regional OM grids
- the calculation of regional SSL grids
- the calculation of regional OHC grids
- the calculation of the global mean of SL and OM grids to get the GMSL and GMOM time series
- the calculation of the global mean of SSL to get the GMSSL time series
- the calculation of the GOHC from the GMSSL
- the calculation of the GOHC from the spatial integration at global scale of OHC grids
- the calculation of the EEI.

For each algorithm, the objectives, the main mathematical statements and the limitations and any comments about the approach are presented.

3.5.2. Preprocessing of SL grids

3.5.2.1. Description

The objective of the preprocessing of SL grid is to modify the temporal and spatial resolutions of SL grids used as input data. Indeed, altimetry data used in MOHeaCAN processing chain is provided by C3S and are given on a daily basis at 0.25x0.25 degrees resolution. As explained in section 3.1, altimetry data need to be downsampled to 3x3 degrees resolution and at the monthly time step to be compared to OM grids.

Moreover, the sea level regional grids from C3S are not corrected from both the glacial isostatic adjustment (GIA) and the elastic effect of the contemporary land ice melting (GRD). To estimate OHC changes, specific corrections must be applied.

3.5.2.2. Mathematical statement

Temporal interpolation

In order to calculate the SL grids on a monthly basis (i.e. to switch from a daily to a monthly temporal resolution), a basic average of the N grids of the month is performed. Cells with default values are not taken into account. The monthly averages are kept for each cell regardless of the number of valid values over the month.

Spatial interpolation

The monthly grids are then computed at a higher spatial resolution: 3x3 degrees instead of 0.25x0.25 degrees. The method applied consists in applying a weighted average to all the cells of the initial grid contained in a 3x3 degrees box, i.e. 144 cells. A weighting grid is calculated to take into account the area of each cell at the resolution of the initial grids 0.25x0.25 degrees.

This grid depends on the latitudes (the surface is reduced for high latitudes) but also on the proportion of water in each cell (e.g. at the approach of the coast). Cells with default values are not taken into account in the calculation of the average.

GIA and GRD corrections

The GIA unstructured ensemble mean grid (see section 2.7) is first sampled on a regular 3 degree resolution grid using linear interpolation. Regional sea level grids are finally corrected from the GIA correction and the GRD correction

$$SL'(x,y,t) = SL(x,y,t) - GIA(x,y) - GRD(x,y)$$

3.5.2.3. Comments/limitations

The temporal and spatial interpolation methods applied are simple. More sophisticated algorithms could be applied to account for data gaps in the time series. Such methods based on the filter approach (e.g. Gaussian filter for spatial interpolation) are planned in future versions of the OHC products. The impact on these improved algorithms is unknown at this time.

With regards to the GIA correction, it is still an area of active research. However the impact at regional scales is mainly significant at high latitudes (e.g. discrepancies can reach 0.5-1 mm/yr) where, for the moment, limited information is provided in the MOHeaCAN product due the application of a restrictive geographical mask based on Argo data (see below for more details).

3.5.3. Preprocessing of OM grids

3.5.3.1. Description

The objective of the preprocessing of OM grid is to modify the spatial resolution of OM grids used as input data. Indeed, gravimetry data used in MOHeaCAN processing chain are provided at 1°x 1° resolution and monthly time step. As explained in section 3.1, gravimetry data need to be downsampled to 3x3 degrees resolution because GRACE(-FO) data do not contain relevant information below about 300 km spatial scale.

3.5.3.2. Mathematical statement

Spatial interpolation

Data from GRACE(-FO) are available worldwide. Only ocean data is kept by applying the land mask. The original OM grids are computed at a higher spatial resolution: 3x3 degrees instead of 1x1 degree. The method applied consists in applying a weighted average to all the cells of the initial grid contained in a 3x3 degrees box, i.e. 9 cells. A weighting grid is calculated to take into account the area of each cell at the resolution of the initial grids 0.25x0.25 degrees. This grid depends on the latitudes (the surface is reduced for high latitudes) but also on the proportion of water in each cell (e.g. at the approach of the coast). Cells with default values are not taken into account in the calculation of the average.

Management of the data gap

The OM data grids contain several gaps due to degradation of the operational capability of GRACE and GRACE-FO and the transition time between the two missions. Those gaps are problematic because a low pass filtering must be performed on the OHC before the calculation of the EEI. That is why an implementation of a gap filling algorithm has been made in the product chain generation. This algorithm is described as follows:

- Calculation of the climatological signal: removal of the trend and calculation of the average for each month of the year
- Removal of the climatological signal over the whole time series
- Cubic approximation of the time series to fill in the gaps
- Adding the climate signal to the whole time series (including the gap)

This gap filling algorithm has been applied at regional scales, i.e for each element of the OM grid.

An important feature brought by the gap algorithm to the OHC-EEI product is a quality flag which distinguishes between months for which there is data from observations and those for which there is data from extrapolation of OM. A more detailed explanation of this quality flag is given in the PUM.

Addition of a high frequency component into the data gaps

The gap-filling algorithm underestimates the part of the signal driven by sub-annual processes. By construction, the high frequency content of the GMOM uncertainty estimates in the data gaps are also underestimated. To deal with that problem, prior to the calculation of the variance-covariance matrix (section 4.4.2.), some modifications were directly made onto the signals of the ensemble of ocean mass solutions. The high frequency related signal component was added to the ensemble signals as follows:

- Application of a 1-year filter onto OM data with prior removal of the annual and semi-annual components of the signal
- Calculation of the standard deviation of the difference between the initial and filtered OM signal
- Stochastic addition with a normal (Gaussian) distribution of this residual standard deviation at the locations where the OM is suffering from a lack of data

Note that this method is applied to all the data gaps on the full time period.

3.5.3.3. Comments/limitations

The spatial interpolation method applied is simple. More sophisticated algorithms could be applied to account for data gaps in the time series. Such methods based on the filter approach (e.g. Gaussian filter for spatial interpolation) are planned in future versions of the OHC products. The impact on these improved algorithms is unknown at this time.

3.5.4. Calculation of regional SSL grids

3.5.4.1. Description

The objective is to calculate the regional SSL grids from SL and OM grids. The relationship between sea level change (SL), ocean mass change (OM) and ocean thermal expansion change (SSL) is expressed by the sea level budget equation:

$$SL = SSL + OM$$

When corrected for changes in ocean mass, sea level change provides an estimate of the thermal expansion of the ocean (SSL).

3.5.4.2. Mathematical statement

The SL grids are obtained from the difference between SL and OM grids at each time step. As SL and OM grids have been preprocessed at same spatial and temporal resolution, the differences between grids is straightforward:

$$SSL(lon, lat, t) = SL(lon, lat, t) - OM(lon, lat, t)$$

For each cell containing a default value in the SL or OM grids, a default value is assigned in the SSL grids.

3.5.4.3. Comments/limitations

Other alternative methodologies are used to derive the steric sea level grids. They rely on in situ data instead of spatial data, mainly from temperature and salinity profiles provided by the Argo network. The advantages and inconvenients of such an approach is presented in (Meyssignac et al., 2019).

Steric sea level is obtained by subtraction of two signals. Some limitations related to this operation can be identified. First, these two are anomalies defined on different reference periods (1992-2012 for altimetry and 2005-2015 for gravimetry). Second, the GIA datasets used to correct the gravimetry signals and the sea level from altimetry are not consistent (three different GIA corrections for the post-processing of gravimetry solutions and one solution for altimetry, see sections 2.2.1 and 2.7). Finally, the dynamical atmospheric correction based on MOG2D model (Carrère and Lyard, 2003, [RD6]) has been removed in altimetry processing whereas only the inverse barometer correction has been applied in gravimetry processing (Blazquez et al., 2018). The impact of this discrepancy must be studied and corrected if needed.

3.5.5. Calculation of regional OHC grids

3.5.5.1. Description

The objective is to calculate the regional OHC grids from SSL grids at the same spatial and temporal resolution. Once the IEEH coefficients are determined at regional scale (grid of constant values over time), SSL changes are translated to OHC changes by dividing them by the IEEH.

3.5.5.2. Mathematical statement

In order to get the ocean heat content (in Joules), we divide all grids of steric sea level changes (m) by the regional IEEH grid ($m.J^{-1}$). The OHC is expressed per unit of area ($J.m^{-2}$), when dividing by the reference surface (see Section 3.2):

$$OHC(lon, lat, t) = \frac{SSL(lon, lat, t)}{surf_{ref} * IEEH(lon, lat)}$$

where $surf_{ref} = 4\pi * (R + h_{TOA})^2$ is defined as the surface of the Earth at the top of the atmosphere, for a reference height of the top of the atmosphere at 20 km altitude ($h_{TOA} = 20.10^3\ m$), with R the radius of the Earth ($R = 6371.10^3\ m$).

It results in monthly OHC changes given on a 3°x3° resolution grid. For each cell containing a default value in the SSL or IEEH grids, a default value is assigned in the OHC grids.

3.5.5.3. Comments/limitations

As mentioned in Section 3.2, the SSL grids describe not only the variation in thermal expansion of sea level but also halosteric effects. It is assumed as a first approximation that the regional OHC variations can be calculated from the SSL grids without accounting for ocean salinity change because sea level expansion is mostly driven by the temperature changes.

The grid containing the regional IEEH coefficients provided was calculated from the temperature and salinity profiles derived from the Argo network (Marti et al., 2021). Consequently, this grid is not defined in coastal areas (with bathymetry less than 700 m) and in high latitudes. This is currently a limitation for calculating the regional OHC over the whole sea surface. In the future, one of the objectives is to find a solution to extrapolate this grid in a realistic way that will allow us to know the variations of the OHC over almost all oceans.

"Altimetry-Gravimetry" methodology provides access to the steric sea level change over the entire water column while the IEEH used to derive the OHC does not consider the effects from the deep oceans (below 2000 m). The impact of this lack of consistency is expected to be small because deep layers are currently less affected by thermal expansion than the surface layers of the ocean.

3.5.6. Calculation of the global mean time series for the GMSL and GMOM

3.5.6.1. Description

The objective is to calculate the global mean time series of SL and OM from SL and OM grids calculated after being preprocessed in space (3x3 degrees) and time (monthly time step).

3.5.6.2. Mathematical statement

At each time step (monthly), the global average (GMSL or GMOM) of each grid (3x3 degrees) is calculated by performing a weighted average taking into account the sea surface of each cell. The weighting grid (w) takes into consideration the surface area of each cell but also the

water/land ratio. Below the mathematical formulation for the GMSL (exactly the same for GMOM):

$$GMSL(t) = \frac{1}{N * N'} \frac{\sum_{i=1}^{N} \sum_{j=1}^{N'} w(lon_i, lat_j) * SL(lon_i, lat_j, t)}{\sum_{i=1}^{N} \sum_{j=1}^{N'} w(lon_i, lat_j)}$$

Moreover, in order to be consistent with the calculation of the regional OHC, a mask where the coefficients of the IEEH grid are defined (corresponding to the availability of Argo data, see Section 3.5.5.3) is first applied before calculating the global average of the grids.

3.5.6.3. Comments/limitations

The GMSL and GMOM time series are calculated on the limited area provided by the IEEH coefficient grid corresponding to the spatial coverage of the Argo network. As the IEEH coefficient grid covers about 84% of the ocean surface, the time series calculation does not represent the full ocean coverage. The impact of this limitation is under investigation.

3.5.7. Calculation of the global mean time series for the GMSSL

3.5.7.1. Description

The objective is to calculate the global mean time series for the GMSSL from the GMSL and GMOM time series. As already mentioned at regional scale, the relationship between the global sea level change (GMSL), the global mean ocean mass change (GMOM) and the global ocean thermal expansion change (GMSSL) is expressed by the sea level budget equation:

$$GMSL = GMSSL + GMOM$$

When corrected for changes in ocean mass, sea level change provides an estimate of the thermal expansion of the ocean.

3.5.7.2. Mathematical statement

The GMSSL is obtained from the difference between the GMSL and GMOM time series at each time step. As GMSL and GMOM time series have been preprocessed at same temporal resolution (monthly), the differences between time series is straightforward:

$$GMSSL(t) = GMSL(t) - GMOM(t), for\ t \in [t_0, t_n]$$

For each time step containing a default value for the GMSL or GMOM time series, a default value is assigned in the GMSSL time series.

3.5.7.3. Comments/limitations

Same as for GMSL and GMOM time series calculation.

3.5.8. Calculation of the global time series for the GOHC from the GMSSL

3.5.8.1. Description

The objective is to calculate the global OHC from the GMSSL time series. Once the EEH coefficient at global scale is determined, global OHC changes are computed by dividing the global mean of the thermal expansion changes by the EEH.

3.5.8.2. Mathematical statement

In order to get the GOHC, the GMSSL (m) is divided by the coefficient of expansion efficiency of heat (global EEH or ε, $m.J^{-1}$). The GOHC is expressed per unit of area ($J.m^{-2}$), when dividing by the reference surface (see Section 3.2):

$$GOHC(t) = \frac{GMSSL(t)}{\varepsilon * surf_{ref}}, for\ t \in [t_0, t_n]$$

where $surf_{ref} = 4\pi * (R + h_{TOA})^2$ is defined as the surface of the Earth at the top of the atmosphere, for a reference height of the top of the atmosphere at 20 km altitude ($h_{TOA} = 20.10^3\ m$), with R the radius of the Earth ($R = 6371.10^3\ m$).

3.5.8.3. Comments/limitations

The GOHC time series can directly be derived from the GMSSL because at global scale the GMSSL is comparable to the global mean thermal expansion of sea level (see Section 3.2).

This calculation can be performed because we made sure of the consistency between the GMSSL time series and ε from (Marti et al., 2021). As mentioned in Section 3.5.7.3, the GMSSL time series is not representative of the full ocean surface, but of the Argo data availability coverage used to compute the IEEH grid and, this Argo-based geomask is the same for the global EEH ε.

As already mentioned in the previous sections, this Argo-based geomask is a limitation since coastal areas and high latitudes are excluded and further improvements are envisaged.

"Altimetry-Gravimetry" methodology provides access to the steric sea level change over the entire water column while the EEH used to derive the OHC does not consider the effects from the deep oceans (below 2000 m). The impact of this lack of consistency is expected to be small because deep layers are currently less affected by thermal expansion than the surface layers of the ocean.

3.5.9. Calculation of the global time series for the GOHC from the OHC grids

3.5.9.1. Description

The objective is to compute the global OHC time series (GOHC) from the OHC grids previously computed at the same time step (monthly). As the OHC is not an integrative variable, the global OHC is not derived from the global average of OHCs as for the GMSL or GMOM time series, but is simply deduced by summing the valid OHC values from each OHC grid of each time step.

3.5.9.2. Mathematical statement

The GOHC ($J.m^{-2}$) time series is the sum of each OHC cell for each OHC grid at each time step (monthly) for valid values only (default values are ignored):

$$GOHC(t) = \sum_{i=1}^{N} \sum_{j=1}^{N'} OHC(lon_i, lat_j, t), for\ t \in [t_0, t_n]$$

3.5.9.3. Comments/limitations

The GOHC time series obtained should be theoretically the same as the GOHC calculated via the global approach (see previous section section 3.5.8). As mentioned in the introduction, the calculation is performed to assess the consistency between both ways to calculate GOHC.

On the other hand, the propagation of uncertainties is, for the moment, carried out only from the global approach. Thus the GOHC calculated from the regional approach does not yet contain the associated uncertainties (see section 4 on uncertainties estimation). It is also for this reason that we have maintained the global approach in the processing chain.

3.5.10. Calculation of the EEI

3.5.10.1. Description

The Global Ocean Heat Uptake (GOHU) corresponds to temporal variations of the GOHC, it represents almost 90% of the EEI. It is therefore simply inferred from the time derivative of the GOHC on a monthly basis. As the high-frequency content of GOHC contains signals which are not related to the EEI (see limitations section), EEI variations cannot be estimated for time scales lower than 2-3 years at this stage of the MOHeaCAN project. By consequence, the GOHC first needs to be filtered-out from signals lower than 3 years before calculating GOHU and after that the EEI. For information, we also provide the EEI deduced after filtering-out signals lower than 2 years and 1 year, in order to conduct more in-depth analyses on the rapid variations of the EEI although they are not representative of climate change to date.

3.5.10.2. Mathematical statement

EEI is calculated from these following steps:

- mean annual and semi-annual cycles are removed from the GOHC time series after estimating these both signals by applying a least square method
- the adjusted GOHC signal is smoothed using a low pass filter (Lanczos) with a cut-off period at λ=3 years for the reference EEI . A 1 year and 2 years cut-off period is also applied to generate EEI containing higher temporal variations but dominated by errors to date (see limitations section).
- GOHU is calculated from the temporal derivative of the filtered and adjusted GOHC time data series:

$$GOHU(t) = \frac{d\,GOHC_{filtred,adjusted}(t)}{dt}, for\ t \in [t_0, t_n]$$

- Since GOHU represent 90% of the EEI, we can obtain the EEI with:

$$EEI(t) = GOHU(t) * \frac{1}{\alpha}, with\ \alpha = 0.9$$

$$EEI \approx \frac{1}{\alpha}\frac{d\,GOHC}{dt}$$

3.5.10.3. Comments/limitations

On the other hand, the high-frequency content of GOHC contains signals which are not related to the EEI imbalance. Firstly, the GOHC contains high-frequency signals (< 2-3 years) which are due to errors in spatial gravimetry measurements but also in altimetry measurements (e.g. phase shift of the annual signals between these measurements). Moreover, the GOHC also contains a residual signal (< 2-3 years) related to the ocean variability at small temporal scale but not related to ocean warming due to climate change. For these reasons it is necessary to filter out these high-frequency signals. At this stage of the study, we recommend filtering this high-frequency content at 3 years, before estimating the EEI and its variations as reliably as possible.

The computation of the temporal derivative is made by applying a central finite difference scheme on the signal:

$$GOHU(t) = \frac{GOHC_{filtred,adjusted}(t+1) - GOHC_{filtered,adjusted}(t-1)}{2*dt}, for\ t \in [t_1, t_{n-1}]$$

Except for $t = t_0$ where we use the forward finite difference scheme and for $t = t_n$ where we use the backward finite difference scheme.

4. Uncertainties calculation and propagation

4.1. Overview

In parallel to the product processing described in the previous section, the uncertainties are calculated and provided for all the global time series: GMSL, GMOM, GMSSL, GOHC and EEI. The proposed approach consists in providing a variance-covariance matrix ($\sum$) of the errors for each time series. Once the variance-covariance matrices are known, the trend uncertainties can be derived for any time-spans over each time series. It is also possible to make it for any other indicators such as the mean, the acceleration or the magnitude of the annual signals for instance. The method is based on the study performed by Ablain et al., 2019 dedicated to the GMSL trend and acceleration uncertainties.

At this stage of the MOHeaCAN project, the uncertainties are not provided at regional scales. Such regional uncertainties have been already provided by Prandi et al., 2020 for the sea level trends and accelerations, but work is still necessary to generalise the approach for other variables, and also to account for the spatial correlation of the errors.

The Figure 5 below describes main steps to propagate the uncertainties from the GMSL and GMOM times series until the GOHC and the EEI . The following subsections described the algorithms developed in detail.

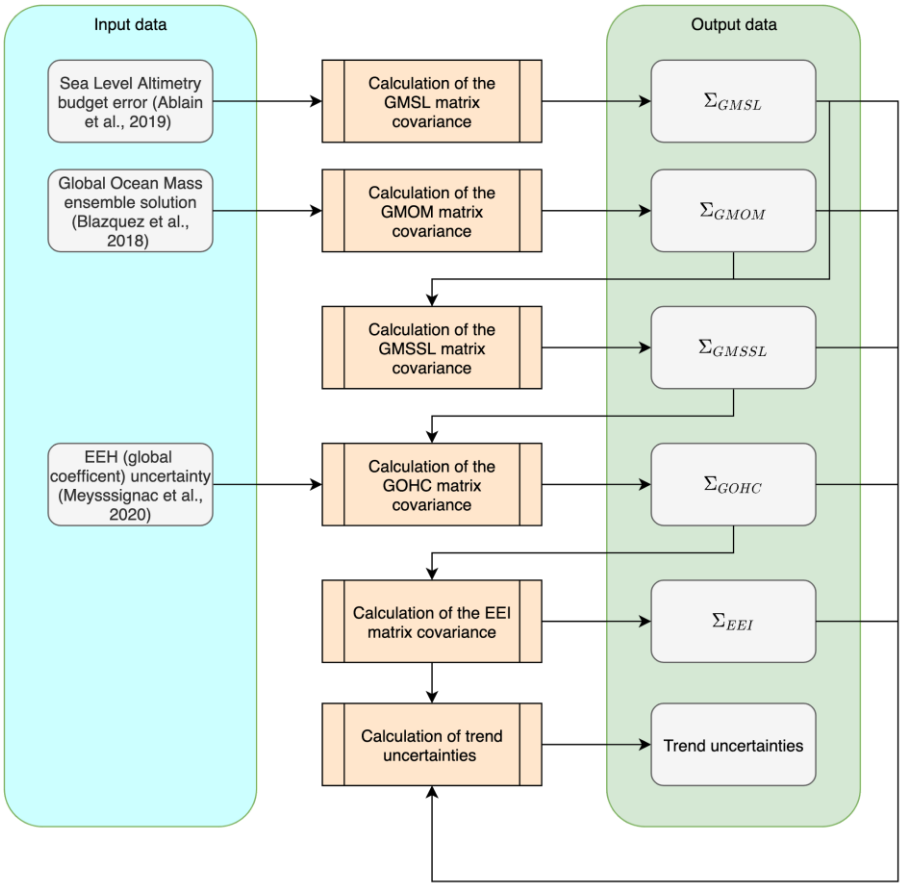

Figure 5 *: Uncertainty calculation and propagation chain*

4.2. Input Data

The input data used are:

- the sea level altimetry error budget given by Ablain et al., (2019) and displayed on table below,
- the ensemble of ocean mass solutions provided by Blazquez et al. (2018) available in NetCDF format file on the LEGOS ftp site [Table 1, RD4].
- land mask (spatial resolution: 1° x 1°)
- the uncertainty of the thermal expansion of heat coefficient provided by Marti et al., (2021): $5.5.10^{-4}\, m.YJ^{-1}$

Source of errors	Error category	Uncertainty level (at 1 σ)
High frequency errors: altimeter noise, geophysical corrections, orbits ...	Correlated errors (λ = 2 months)	σ = 1.7 mm for TOPEX period σ = 1.5 mm for Jason-1 period. σ = 1.2 mm for Jason-2/3 period.
Medium frequency errors: geophysical corrections, orbits ...	Correlated errors (λ = 1 year)	σ = 1.3 mm for TOPEX period σ = 1.2 mm for Jason-1 period. σ = 1 mm for Jason-2/3 period.
Large frequency errors: wet troposphere correction	Correlated errors (λ = 5 years)	σ = 1.1 mm over all the period (⇔ to 0.2 mm/yr for 5 years)
Large frequency errors: orbits (Gravity fields)	Correlated errors (λ = 10 years)	σ = 1.12 mm over TOPEX period (no gravimetry data on this period) σ = 0.5 mm over Jason period (⇔ to 0.05 mm/yr for 10 years)
Altimeter instabilities on TOPEX-A and TOPEX-B	Drift error	δ = 0.7 mm/yr on TOPEX-A period δ = 0.1 mm/yr on TOPEX-B period
Long-term drift errors: orbit (ITRF) and GIA	Drift error	δ = 0.12 mm/yr over 1993-2017
GMSL bias errors to link altimetry missions together	Bias errors	D = 2 mm for TP-A/TP-B D = 0.5 mm for TP-B/J1, J1/J2, J2/J3.

Table 3 *: Altimetry GMSL error budget given at 1-sigma*

4.3. Output Data

Errors are characterised with the following variance-covariance matrices:

- Σ_{GMSL},$\Sigma_{GMOM}$and $\Sigma_{GMSSL}$for the global mean SL, OM and SSL time series
- $\Sigma_{GOHC}$for the global OHC time series
- $\Sigma_{EEI}$for the EEI for several GOHC low-pass filtering periods (1 year-filtered, 2 year-filtered and, 3 year-filtered)

4.4. Retrieval methodology

4.4.1. Calculation of the GMSL covariance matrix

4.4.1.1. Description

The objective is to calculate the error variance-covariance matrix of the GMSL time series (Σ_{GMSL}) for the time period of the study. $\Sigma_{GMSL}$is deduced from the sea level error budget described in Table 3.

4.4.1.2. Mathematical statement

We assumed that all error sources shown in Table 4 are independent one to each other. Thus the matrix is the sum of the individual variance-covariance matrices of each error source in the sea level error budget:

$$\Sigma_{GMSL} = \sum_{i=1}^{n} \Sigma_{Error_i}$$

Each matrix is calculated from a large number of random draws (> 1000) of simulated error signal where the correlation is modelled with a Gaussian attenuation based on the wavelength (λ) of the errors: $e^{-\frac{1}{2}(\frac{t}{\lambda})^2}$.

4.4.1.3. Comments/Limitations

This matrix is based on the current knowledge of altimetry measurement errors. As the altimetry record increases in length with new altimeter missions, the knowledge of the altimetry measurement also increases and the description of the errors improves. Consequently, the error variance-covariance matrix is expected to change and improve in the future – hopefully with a reduction of measurement uncertainty in new products.

It is also important to note that the error budget approach applied here to derive the variance-covariance matrix is conservative. In other words, sea level altimetry errors may be overestimated with respect to reality. Further studies are planned to analyse the sensitivity of this error budget on the GOHC and EEI uncertainties.

4.4.2. Calculation of the GMOM covariance matrix

4.4.2.1. Description

The objective is to calculate the error variance-covariance matrix of the GMOM time series (Σ_{GMOM}) for the time period of the study. $\Sigma_{GMOM}$is derived from a GMOM ensemble deduced from the ensemble of ocean mass solutions provided by Blazquez et al. (2018), containing 216 GRACE(-FO) grids datasets.

4.4.2.2. Mathematical statement

The OM data from GRACE(-FO) are available worldwide. Only ocean data are kept by applying the land mask. At each time step (monthly), the global average of each ocean mass solution grid (1x1 degree) is calculated by performing a weighted average taking into account the sea

surface of each cell. The weighting grid (w) takes into consideration the surface area of each cell but also the water/land ratio.

The resulting GMOM ensemble solutions contains n temporal vectors noted hereafter X_i for i=1 from 1 to n. The variance-covariance matrix (Σ_{GMOM}) is the matrix whose entry is the covariance:

$$\Sigma_{GMOM}(i,j) = cov(X_i, X_j) = E[(X_i - E[X_i])(X_j - E[X_j])]$$

where E is the mean operator.

Addition of a block matrix in the variance-covariance matrix into the data gap

The gap-filling algorithm (described in section 3.5.3.2.) underestimated the part of the signal driven by sub-annual processes. Adding a high frequency component (section 3.5.3.2.) to the ensemble with a stochastic method allowed us to correct a part of this high frequency signal, inducing an increase of the coefficients located on the diagonal of the variance-covariance matrix (Σ_{GMOM}). However, the non-diagonal terms of Σ_{GMOM} characterizing the time correlated errors (for example those linked with inter-annual variability) are still underestimated. In order to obtain more realistic uncertainties into the data gaps, an empirical a posteriori approach is developed, based on the following steps:

- identification of a period of the same duration as the period of the data gap
- extraction of the terms of the block variance-covariance matrix on this period
- addition of the matrix taken on the block matrix of the period to be reconstructed

GMOM uncertainties based on the variance-covariance matrix are now taking into account the time correlated errors. Note that this method is just applied to the main data gap corresponding to the transition between GRACE and GRACE-FO (2016-2018).

4.4.2.5. Comments/Limitations

The ensemble mean provided by Blazquez et al. (2018) contains 216 solutions which is a important number of solutions to calculate Σ_{GMOM}. However the mathematical formulation above assumes a normal distribution of the different GMOM solutions. In practice, it is not fully the case. Thorough investigations must be performed to analyse the impact of this approximation.

In contrast to altimetric sea level errors, the ensemble error approach applied here to derive a variance-covariance matrix could be considered as an optimistic view of the GMOM error description. This means that GMOM uncertainties could be underestimated.

4.4.3. Calculation of the GMSSL covariance matrix

4.4.3.1. Description

The objective is to compute the variance-covariance matrix of the GMSSL errors (Σ_{GMSSL}). As GMSSL is obtained by calculating the differences between GMSL and GMOM, Σ_{GMSSL} is obtained by summing the variance-covariance matrices of the errors of GMSL and GMOM. Indeed, since the errors of the two data sets can be considered independent, the errors are additive.

4.4.3.2. Mathematical statement

Σ_{GMSSL} is the sum of Σ_{GMSL} and Σ_{GMOM}.

4.4.3.3. Comments/Limitations

The proposed method for propagating GMSL and GMOM errors does not take into account the errors of the C3S grids and GRACE data collocation method (spatially and temporally). However, these errors are assumed to be quite small.

4.4.4. Calculation of the GOHC covariance matrix

4.4.4.1. Description

The objective is to calculate the variance-covariance matrix of the GOHC errors (Σ_{GOHC}). The errors from GMSSL time series are propagated to the GOHC time series taking into account the relationship between the GOHC and GMSSL via the global expansion efficiency of heat coefficient (ε or global EEH) and its uncertainty (e_ϵ). $\Sigma_{GOHC}$is inferred from Σ_{GMSSL} from the following relationship (see details in next subsection).

$$GOHC(t) = \frac{GMSSL\ (t) \pm e_{GMSSL}(t)}{\epsilon \pm e_\epsilon}$$

4.4.4.2. Mathematical statement

In case of two uncorrelated scalar variables a and b, with a respective uncertainty e_a and e_b, the error propagation division follows the ensuing relationship (Taylor, 1997, equation 3.8):

$$(e_{\frac{a}{b}})^2 = \left(\frac{1}{b}\right)^2 * \left[{e_a}^2 + \left(e_b * \frac{a}{b}\right)^2\right]$$

In our case:

- a= GMSSL(t) and ϵ_a is $e_{GMSSL}(t)$
- b= global EEH (noted ϵ) and ϵ_b is given by e_ϵ
- $\frac{a}{b} = \frac{GMSSL(t)}{GEEH} = GOHC(t)$

Thus with these notations, the first equation becomes:

$$\left(e_{GOHC(t)}\right)^2 = \frac{1}{\epsilon^2} * (e_{GMSSL}(t))^2 + \left(\frac{e_\epsilon}{\epsilon}\right)^2 * (GOHC(t))^2$$

which can be written in matricial notation with the variance-covariance matrices Σ_{GOHC} and Σ_{GMSSL} (containing the uncertainties ${e_{GOHC}}^2$ and ${e_{GMSSL}}^2$ respectively) as follows:

$$\Sigma_{GOHC} = \frac{1}{\epsilon^2}\Sigma_{GMSSL} + \left(\frac{e_\epsilon}{\epsilon}\right)^2 GOHC * GOHC^t$$

4.4.4.3. Comments/Limitations

The mathematical formalism proposed for the propagation of errors from the GMSSL to the GOHC shows that the errors of the GOHC depend both on the uncertainty of the value of the EEH coefficient and on the value of the coefficient itself. When analysing the impact of changing this coefficient and its uncertainty (from Levitus et al., 2012/Kuhlbrodt and Gregory, 2012 to Marti et al., 2021), we found that this significantly reduced GOHC and EEI uncertainties.

4.4.5. Calculation of the EEI covariance matrix

4.4.5.1. Description

The objective is to compute the variance-covariance matrix of errors of the EEI (Σ_{EEI}) from Σ_{GOHC}. Contrary to the error propagation for the GMSSL or the GOHC where a formal approach has been specified, an empirical approach is proposed here where a set of solutions of GOHC errors (> 1000) is generated in a random way from Σ_{GOHC}. Therefore, the set of error solutions of the corresponding EEI is computed as described in the algorithm "Calculation of the EEI ". Then the variance-covariance matrix of EEI is computed from this set following the algorithm described in "Calculation of the GMOM covariance matrix".

4.4.5.2. Mathematical statement

Each random solution of GOHC errors is a vector following a Gaussian vector of mean 0 and covariance matrix Σ_{GOHC}: $N(0,\Sigma_{GOHC})$. They are obtained by the product of the Cholesky decomposition of Σ_{GOHC} (which is semi positive-definite matrix by construction), and a random vector following (R_k) a Gaussian vector of mean 0 and covariance matrix the identity: $N(0,I)$.

Σ_{GOHC} can be written by Cholesky:

$$\Sigma_{GOHC} = AA^t$$

and each GOHC error vector (e_k) equals:

$$e_k = AR^t{}_k$$

Each e_k is then filtered by a low-pass filter (Lanczos) with cut-off period λ:

$$\widehat{e_k} = F_\lambda(e_k)$$

And the OHU variance-covariance matrix corresponds to the following calculation:

$$\Sigma_{OHU}(i,j) = cov(\widehat{e_{k_i}}, \widehat{e_{k_j}}) = E[(\widehat{e_{k_i}} - E[\widehat{e_{k_i}}])(\widehat{e_{k_j}} - E[\widehat{e_{k_j}}])]$$

where E is the mean operator.

The final operation applies consists in applying the formulation from Section 3.5.10.2. for the division of the GOHU by the α fraction. Σ_{EEI} is obtained simply from Σ_{GOHU} neglecting any errors in α:

$$\Sigma_{EEI}(i,j) = \frac{1}{\alpha^2}\Sigma_{OHU}(i,j), with\ \alpha = 0.9$$

4.4.5.3. Comments/Limitations

$\Sigma_{EEI}$is provided for λ=3 years for the reference filtering period to calculate EEI, however for more thorough studies analyses Σ_{EEI} is also provided for λ=1 and 2 years.

4.4.6. Calculation of trend uncertainties

4.4.6.1. Description

The objective is to calculate the trend uncertainty, adjusting a polynomial of degree 1 by an ordinary least square (OLS) method taking into account the error variance-covariance matrix for the calculation of the uncertainty.

4.4.6.2. Mathematical statement

The ordinary least square (OLS) regression method is used in this study. The estimator of β with the OLS approach is noted:

$$\hat{\beta} \sim (X^t X)^{-1} X^t y$$

where y is the vector containing the observations (e.g. GMSL, GOHC, ...) and X the vector containing the dates of the observations.

The uncertainty in the trend estimates takes into account the correlated errors of the observations (y). So, the error is integrated into the trend uncertainty estimation. Taking into account the variance-covariance matrix (Σ) , the estimator of β becomes:

$$\hat{\beta} = N(\beta, (X^t X)^{-1}(X^t \Sigma X)(X^t X)^{-1})$$

4.4.6.3. Comments/Limitations

The proposed approach is also applicable for any other adjusted variables. For instance, the acceleration of the time series can be calculated from the adjustment of a polynomial of degree 2 ($a_0 + a_1 X + a_2 X^2$) where the acceleration (a) is given by $a = 2a_2$. The uncertainty acceleration is calculated applying the same mathematical formalism described previously for the trend.

5. References

- Ablain, M., Cazenave, A., Larnicol, G., Balmaseda, M., Cipollini, P., Faugère, Y., Fernandes, M. J., Henry, O., Johannessen, J. A., Knudsen, P., Andersen, O., Legeais, J., Meyssignac, B., Picot, N., Roca, M., Rudenko, S., Scharffenberg, M. G., Stammer, D., Timms, G., and Benveniste, J.: Improved sea level record over the satellite altimetry era (1993–2010) from the Climate Change Initiative project, Ocean Sci., 11, 67–82, https://doi.org/10.5194/os-11-67-2015, 2015.
- Ablain, M., Meyssignac, B., Zawadzki, L., Jugier, R., Ribes, A., Cazenave, A., and Picot, N.: Error variance-covariance matrix of global mean sea level estimated from satellite altimetry (TOPEX, Jason 1, Jason 2, Jason 3), https://doi.org/10.17882/58344, 2018.
- Ablain, M., Meyssignac, B., Zawadzki, L., Jugier, R., Ribes, A., Spada, G., Benveniste, J., Cazenave, A., and Picot, N.: Uncertainty in satellite estimates of global mean sea-level changes, trend and acceleration, Earth Syst. Sci. Data, 11, 1189–1202, https://doi.org/10.5194/essd-11-1189-2019, 2019.
- Blazquez, A., Meyssignac, B., Lemoine, J., Berthier, E., Ribes, A., and Cazenave, A.: Exploring the uncertainty in GRACE estimates of the mass redistributions at the Earth surface: implications for the global water and sea level budgets, Geophys. J. Int., 215, 415–430, https://doi.org/10.1093/gji/ggy293, 2018.
- Carrère, L. and Lyard, F.: Modeling the barotropic response of the global ocean to atmospheric wind and pressure forcing - comparisons with observations, Geophys. Res. Lett., 30, https://doi.org/10.1029/2002GL016473, 2003.
- Church, J. A., White, N. J., Konikow, L. F., Domingues, C. M., Cogley, J. G., Rignot, E., Gregory, J. M., Broeke, M. R. van den, Monaghan, A. J., and Velicogna, I.: Revisiting the Earth's sea-level and energy budgets from 1961 to 2008, Geophys. Res. Lett., 38, https://doi.org/10.1029/2011GL048794, 2011.
- Frederikse, T., Riva, R. E. M., and King, M. A.: Ocean Bottom Deformation Due To Present-Day Mass Redistribution and Its Impact on Sea Level Observations, Geophys. Res. Lett., 44, 12,306-12,314, https://doi.org/10.1002/2017GL075419, 2017.
- Hansen, J., Sato, M., Kharecha, P., and von Schuckmann, K.: Earth's energy imbalance and implications, Atmospheric Chem. Phys., 11, 13421–13449, https://doi.org/10.5194/acp-11-13421-2011, 2011.
- Kuhlbrodt, T. and Gregory, J. M.: Ocean heat uptake and its consequences for the magnitude of sea level rise and climate change, Geophys. Res. Lett., 39, https://doi.org/10.1029/2012GL052952, 2012.
- L'Ecuyer, T. S., Beaudoing, H. K., Rodell, M., Olson, W., Lin, B., Kato, S., Clayson, C. A., Wood, E., Sheffield, J., Adler, R., Huffman, G., Bosilovich, M., Gu, G., Robertson, F., Houser, P. R., Chambers, D., Famiglietti, J. S., Fetzer, E., Liu, W. T., Gao, X., Schlosser, C. A., Clark, E., Lettenmaier, D. P., and Hilburn, K.: The Observed State of the Energy Budget in the Early Twenty-First Century, J. Clim., 28, 8319–8346, https://doi.org/10.1175/JCLI-D-14-00556.1, 2015.
- Levitus, S., Antonov, J. I., Boyer, T. P., Locarnini, R. A., Garcia, H. E., and Mishonov, A. V.: Global ocean heat content 1955-2008 in light of recently revealed instrumentation problems: GLOBAL OCEAN HEAT CONTENT, Geophys. Res. Lett., 36, n/a-n/a, https://doi.org/10.1029/2008GL037155, 2009.
- Levitus, S., Antonov, J. I., Boyer, T. P., Baranova, O. K., Garcia, H. E., Locarnini, R. A., Mishonov, A. V., Reagan, J. R., Seidov, D., Yarosh, E. S., and Zweng, M. M.: World ocean

heat content and thermosteric sea level change (0–2000 m), 1955–2010, Geophys. Res. Lett., 39, https://doi.org/10.1029/2012GL051106, 2012.

- Loeb, N. G., Doelling, D. R., Wang, H., Su, W., Nguyen, C., Corbett, J. G., Liang, L., Mitrescu, C., Rose, F. G., and Kato, S.: Clouds and the Earth's Radiant Energy System (CERES) Energy Balanced and Filled (EBAF) Top-of-Atmosphere (TOA) Edition-4.0 Data Product, J. Clim., 31, 895–918, https://doi.org/10.1175/JCLI-D-17-0208.1, 2018.
- Marti, F., Blazquez, A., Meyssignac, B., Ablain, M., Barnoud, A., Fraudeau, R., Jugier, R., Chenal, J., Larnicol, G., Pfeffer, J., Restano, M., and Benveniste, J.: Monitoring the ocean heat content change and the Earth energy imbalance from space altimetry and space gravimetry, Earth Syst. Sci. Data Discuss., 1–32, https://doi.org/10.5194/essd-2021-220, 2021.
- Melet, A. and Meyssignac, B.: Explaining the Spread in Global Mean Thermosteric Sea Level Rise in CMIP5 Climate Models*, J. Clim., 28, 9918–9940, https://doi.org/10.1175/JCLI-D-15-0200.1, 2015.
- Meyssignac, B., Boyer, T., Zhao, Z., Hakuba, M. Z., Landerer, F. W., Stammer, D., Köhl, A., Kato, S., L'Ecuyer, T., Ablain, M., Abraham, J. P., Blazquez, A., Cazenave, A., Church, J. A., Cowley, R., Cheng, L., Domingues, C. M., Giglio, D., Gouretski, V., Ishii, M., Johnson, G. C., Killick, R. E., Legler, D., Llovel, W., Lyman, J., Palmer, M. D., Piotrowicz, S., Purkey, S. G., Roemmich, D., Roca, R., Savita, A., Schuckmann, K. von, Speich, S., Stephens, G., Wang, G., Wijffels, S. E., and Zilberman, N.: Measuring Global Ocean Heat Content to Estimate the Earth Energy Imbalance, Front. Mar. Sci., 6, https://doi.org/10.3389/fmars.2019.00432, 2019.
- Prandi, P., Meyssignac, B., Ablain, M., Spada, G., and Ribes, A.: How reliable are local sea level trends observed by satellite altimetry ?, Prep., 2020.
- Russell, G. L., Gornitz, V., and Miller, J. R.: Regional sea level changes projected by the NASA/GISS Atmosphere-Ocean Model, Clim. Dyn., 16, 789–797, https://doi.org/10.1007/s003820000090, 2000.
- von Schuckmann, K., Palmer, M. D., Trenberth, K. E., Cazenave, A., Chambers, D., Champollion, N., Hansen, J., Josey, S. A., Loeb, N., Mathieu, P.-P., Meyssignac, B., and Wild, M.: An imperative to monitor Earth's energy imbalance, Nat. Clim. Change, 6, 138, 2016.
- von Schuckmann, K., Cheng, L., Palmer, M. D., Hansen, J., Tassone, C., Aich, V., Adusumilli, S., Beltrami, H., Boyer, T., Cuesta-Valero, F. J., Desbruyères, D., Domingues, C., García-García, A., Gentine, P., Gilson, J., Gorfer, M., Haimberger, L., Ishii, M., Johnson, G. C., Killick, R., King, B. A., Kirchengast, G., Kolodziejczyk, N., Lyman, J., Marzeion, B., Mayer, M., Monier, M., Monselesan, D. P., Purkey, S., Roemmich, D., Schweiger, A., Seneviratne, S. I., Shepherd, A., Slater, D. A., Steiner, A. K., Straneo, F., Timmermans, M.-L., and Wijffels, S. E.: Heat stored in the Earth system: where does the energy go?, Earth Syst. Sci. Data, 12, 2013–2041, https://doi.org/10.5194/essd-12-2013-2020, 2020.
- Spada, G. and Melini, D.: On Some Properties of the Glacial Isostatic Adjustment Fingerprints, Water, 11, 1844, https://doi.org/10.3390/w11091844, 2019.
- Taylor, J. R.: An Introduction to Error Analysis: The Study of Uncertainties in Physical Measurements, 2nd ed., University Science Books, 344 pp., 1997.
- Trenberth, K. E., Fasullo, J. T., and Balmaseda, M. A.: Earth's Energy Imbalance, J. Clim., 27, 3129–3144, https://doi.org/10.1175/JCLI-D-13-00294.1, 2014.
- Wahr, J., Swenson, S., Zlotnicki, V., and Velicogna, I.: Time-variable gravity from GRACE: First results: TIME-VARIABLE GRAVITY FROM GRACE, Geophys. Res. Lett., 31, n/a-n/a, https://doi.org/10.1029/2004GL019779, 2004.